Quantum and Thermal Dispersion Forces: Application to Graphene Nanoribbons

D. Drosdoff and Lilia M. Woods
Department of Physics, University of South Florida, Tampa, Florida 33620, USA
(Received 25 June 2013; published 14 January 2014)

The van der Waals dispersion force between graphene nanoribbons is investigated. For this purpose, a nonretarded Lifshitz-like formula for parallel 1D systems is presented within the random phase approximation. Using the response properties of the ribbons from a tight binding model, it is found that the qualitative behavior of the force is similar to the one between two insulating 1D systems. On the other hand, the quantum mechanical van der Waals force can become thermal in nature when the nanoribbons have sufficiently strong chemical potential. It is found that this tuning capability is due to the unique dielectric properties of graphene nanoribbons. Results for other typical 1D materials are also presented, which enable building a better understanding of this ubiquitous force at reduced dimensions.

DOI: 10.1103/PhysRevLett.112.025501 PACS numbers: 61.48.Gh, 34.20.Cf, 78.67.Uh, 81.05.ue

Introduction.—The discovery of graphene, a single layer of graphite, has lead to significant technological breakthroughs and exciting new areas of research [1]. Advances towards graphene devices have brought special attention to how graphene and its derivatives interact with each other and with other materials [2]. At the submicron scale, van der Waals (vdW) forces become particularly important due to their long-ranged dispersive nature and nonadditivity. Progress has been made in overcoming computational challenges as first principle methods have been developed to quantify these features [3–5]. Analytical efforts have also shown that the unique properties of graphene affect the vdW interaction in profound ways. For example, unlike most systems at room temperature, the interaction is dominated by thermal fluctuations wherein quantum mechanical effects are negligible [6], even at scales down to 50 nm. Also, the force can be modulated significantly via the graphene chemical potential or by inducing a band gap, which is typically not observed in other systems [7–10]. The first measurements of Casimir-vdW forces between graphene and substrates have also been reported [11].

Graphene nanoribbons (GNRs), strips of graphene, have recently received significant interest [12]. This is largely motivated by the finite energy gap originating from the size constraints, which makes GNRs more suitable for logic nanodevices [13]. Although the vdW interaction is just as important for GNRs as for graphene, the investigation of the force for ribbons has received a lot less attention. Recently, however, there has been a rising interest in 1D Casimir-vdW forces [14–16], whereupon these forces are calculated between metallic and dielectric wires. Although these works provide insight into 1D dispersive interactions, applying their methods for general systems and taking into account the relevant dispersive properties is not straightforward.

Besides understanding the effects of dimensionality and materials properties, the role of temperature (T) on dispersive interactions has been a long-standing issue [17,18]. In addition to the always present quantum mechanical fluctuations, a finite T induces thermal fluctuations. Decoupling and quantifying the thermal and quantum mechanical fluctuations is difficult for typical metals and dielectrics. Recent experiments have reported measurements of the thermal force in the μm range via torsion pendulum apparatus [17]. However, other researchers point out that these results need further evaluations in light of large experimental errors, different dielectric response models, and application of the proximity force theorem [18]. Therefore, finding suitable materials to bring resolution to this debate is highly desirable.

This Letter presents a formalism, based on the random phase approximation (RPA), which gives a Lifshitz-like formula for vdW interactions between 1D structures. We apply this formalism to calculate the force between two GNRs using explicit expressions for their electronic and dielectric properties. We emphasize the quantum mechanical and thermal regimes and identify how the dimensionality and chemical potential affect the strength and distance dependence of the force. We show that the GNR force exhibits transitions from quantum mechanical to thermal by changing the chemical potential. This constitutes major progress in identifying a system, which can potentially be used by experimentalists to tune the interaction in an effective manner. Given the fact that vdW forces are often the cause for stiction between components of microdevices, our study is certainly advantageous for the development of graphene-based electronics. Results for other 1D systems are also given, which enables one to identify common and unique characteristics affecting the vdW force between GNRs.

The van der Waals force.— The system under consideration consists of two ribbons, modeled as infinitely thin, infinitely long strips as shown in Fig 1(a). The nonretarded vdW force [19] is obtained from the average product of the electron density fluctuations, $n_{1,2}$, for each ribbon and the Coulomb interaction energy [6]. The force per unit length is found as

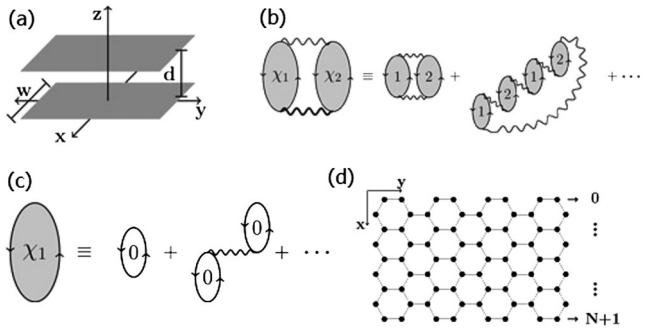

FIG. 1. (a) Two infinitely thin, infinitely long, strips of width w separated by a distance d. (b) Diagrammatic representation of the RPA for the vdW force between two materials with responses $\chi_{1,2}$. (c) Diagrams for the RPA response for each material, where the bare polarization χ_0 is denoted as 0. (d) An armchair GNR of width $w = (N+1)a/2$, where N is the total number of the armchaired C lines and a is the graphene lattice constant.

$$f = -\int_{-w/2}^{w/2} dx_1 \int_{-w/2}^{w/2} dx_2 \int \frac{dq}{2\pi} \times \frac{\partial}{\partial d}[v(|x_1 - x_2|, q, d)]\langle n_1(x_1, q) n_2(x_2, -q)\rangle, \quad (1)$$

where $v(x, q, d) = 2e^2 K_0(|q|\sqrt{x^2 + d^2})$, K_0 is the zeroeth order modified Bessel function of the second kind, and e is the electron charge. The wave vector q is directed along the common axial y direction [Fig. 1(a)].

The equal time density-density correlator, $\langle n_1(x_1, q) n_2(x_2, -q)\rangle$, may be found using finite temperature Green's function techniques [20]. It is related to the polarization χ of the system,

$$\begin{aligned}\chi(\mathbf{r}_1, \tau_1, \mathbf{r}_2, \tau_2) &= \langle T_\tau[n_1(\mathbf{r}_1, \tau_1) n_2(\mathbf{r}_2, \tau_2)]\rangle \\ &\quad - \langle n_1(\mathbf{r}_1, \tau_1)\rangle\langle n_2(\mathbf{r}_2, \tau_2)\rangle \\ &= -G(\mathbf{r}_1, \tau_1; \mathbf{r}_2, \tau_2) G(\mathbf{r}_2, \tau_2; \mathbf{r}_1, \tau_1), \quad (2)\end{aligned}$$

where T_τ is the time ordered product operator with τ being an imaginary time parameter and G is the two-point Green's function. The density-density correlator is evaluated via Wick's theorem, generating a series of two-point correlator products. Further, we utilize the RPA, which corresponds to calculating those correlators represented by the bubble diagrams, shown in Fig. 1(b). The RPA is a good approximation for the collective screening effects for most materials, including graphene and related nanostructures [21]. Averaging over the individual density fluctuations $\langle n_{1,2}(\mathbf{r}_{1,2}, \tau_{1,2})\rangle$ yields zero.

We consider the case of two narrow ribbons with translational symmetry along the axial direction where $d \gg w$. The longitudinal response for this 1D system is given by $\chi(\mathbf{r}, \tau, \mathbf{r}', \tau') = \chi(y - y', \tau, \tau')$. After performing a Fourier transformation along y, one obtains

$$\chi(q, d) = k_B T \sum_l \chi_1(q, i\omega_l) W(q, i\omega_l, d) \chi_2(q, i\omega_l), \quad (3)$$

$$\chi_1(q, \omega_l) = \chi_2(q, \omega_l) = \chi_0(q, \omega_l)/[1 - v(q)\chi_0(q, \omega_l)], \quad (4)$$

$$W(q, \omega_l, d) = v(q, d)/[1 - \chi_1(q, \omega_l) v^2(q, d) \chi_2(q, \omega_l)], \quad (5)$$

where $\omega_l = 2\pi l k_B T/\hbar$ are the Matsubara frequencies, $v(q, d) = 2e^2 w K_0(|q|d)$. The Coulomb potential is often approximated [15] by its dominant term $v(q) = -2e^2 \ln(|q|w)$ for typical metals or dielectrics at small d. The response for each structure $\chi_{1,2}$ (taken to be identical here) is also calculated via the RPA, meaning that χ_0 corresponds to the bare polarization shown in Fig. 1(c).

The above results enable one to write the vdW force per unit length in the following way:

$$\begin{aligned} f &= -2k_B T {\sum_{l=0}}' \int_0^\infty \frac{dq}{\pi} \frac{\partial v(q, d)}{\partial d} \frac{1}{v(q, d)} \\ &\quad \times \left(\frac{1}{\left[\frac{v(q)}{v(q,d)}\right]^2 \frac{1}{\rho_B(q, i\omega_l)^2} - 1} \right), \\ \rho_B(q, i\omega_l) &= \frac{\chi_0(q, i\omega_l)}{1/v(q) - \chi_0(q, i\omega_l)}, \end{aligned} \quad (6)$$

where the prime indicates the $l = 0$ term is multiplied by $1/2$. Equation (6) is a Lifshitz-like expression for the interaction when retardation is not taken into account. It gives a straightforward way to calculate the vdW force between 1D structures in terms of their macroscopic response properties. It requires knowledge of χ_0, which depends on the electronic structure and it corresponds to the longitudinal response of the system. Also note that ρ_B is a unitless coefficient.

This formalism is now applied to calculate the vdW force between some typical materials. The Coulomb potential is approximated by $v(q) = -2e^2 \ln(|q|w)$, which helps us obtain the results summarized in Table I. Consider two 1D insulators, described by a Drude-Lorentz $\chi_0 = -q^2 n_{1D}/$

TABLE I. Approximate vdW forces for 1D materials

1D materials	Force per unit length
Metals	$-\frac{\hbar}{8\pi d^3}\sqrt{\frac{n_{1D}e^2}{m}}\frac{1}{[2\ln(d/w)]^{3/2}}$
Insulators	$-\frac{135\pi}{4096}\frac{\hbar}{\omega_0^3}\left(\frac{n_{1D}e^2}{m}\right)^2\frac{1}{d^6}$
$\sigma = \text{const}$	$-\frac{3\hbar\sigma}{128}\frac{1}{d^4\ln(d/w)}$
Thermal	$-\frac{\pi k_B T}{64}\frac{1}{[d\ln(d/w)]^2}$

$m(\omega_0^2-\omega^2)$, with n_{1D} being the 1D particle density, m being the carrier effective mass, and ω_0 the optical transition frequency. In this case, we find that $f\sim 1/d^6$. For metals, $\omega_0\to 0$ in the Drude-Lorentz response. It is obtained that $f\sim[d\sqrt{\ln(d/\mathrm{w})}]^{-3}$. Both characteristic behaviors agree with previous results found via other methods [14]. However, the strength of the Lifshitz formula approach is that it provides analytical expressions which may show additional characteristics influencing the strength of the force. Hypothetical 1D materials with $\sigma=$ const are also considered. Such materials have the similar Dirac nature carriers as graphene, but they are one dimensional [22]. In this case, $f\sim d^{-4}\ln(d/\mathrm{w})^{-1}$ as opposed to graphene, whose force per unit area has a distance dependence of $\sim d^{-4}$ [14].

GNR response function.—The ribbons from Fig. 1(a) are taken to be armchaired with structure and nomenclature shown in Fig. 1(d).The GNR dielectric response is determined by the optical transitions between valence and conduction bands, originating from the finite width, according to a set of selection rules [23]. The energy of the conduction and valence states, denoted as $s=\pm$, respectively, is calculated using a nearest-neighbor tight binding model. We take into account the energy levels closest to the Fermi level for which the small q approximation is valid. In this case, the energy is given by

$$E_{n,s}(q)=s\hbar v_0\sqrt{k_n^2+q^2}, \tag{7}$$

where $v_0=\sqrt{3}at_0/(2\hbar)$ is the graphene Fermi velocity, $t_0=3$ eV is the nearest neighbor hopping integral, and $a=2.46$ Å is the graphene lattice constant. Also, $k_n=n\pi/\mathrm{w}-4\pi/3a$ with n counting the ribbon substates. The narrow ribbons are essentially semiconductors with a width dependent energy gap E_g [24].

The calculation of the GNR RPA response, shown in Fig. 1(c), requires a multiband model. For a diagram with p bubbles,

$$\chi^p(x,x',q,\omega)=\frac{1}{\mathrm{w}^{2p}}\sum_{[n_p,n_p',s_p,s_p']}\chi_0^{nn_1,ss_1}(q,\omega)v_{nn_1n_1'n_2}(q)\chi_0^{n_2n_2',s_2s_2'}(q,\omega)\ldots v_{n_{(p-1)}n_pn_p'n'}(q)\chi_0^{n_p'n',s_p's'}\cos[(k_n-k_{n'})x]\cos[(k_n-k_{n'})x'], \tag{8}$$

$$v_{nmn'm'}(q)=2e^2\int_0^{\mathrm{w}}dx_1\int_0^{\mathrm{w}}dx_2K_0(q|x-x'|)\cos[(k_n-k_m)x_1]\cos[(k_{n'}-k_{m'})x'], \tag{9}$$

$$\chi_0^{nn',ss'}(q,\omega)=\frac{g}{L}\sum_{k_y}\frac{f[E_{n,s}(k_y+q)-\mu]-f[E_{n',s'}(k_y)-\mu]}{E_{n,s}(k_y+q)-E_{n',s'}(k_y)-\hbar\omega}\times J_{nn',ss'}(k_y,q), \tag{10}$$

where $[\ldots]$ gives the sum over integers $1\ldots p$, and g is the electron spin degeneracy. Also, $f(E_{n,s}-\mu)$ is the Fermi-Dirac distribution and μ is the chemical potential. The wave functions for the (n,s) states are not given here as they can be found in Ref. [25]. The wave functions overlap integral is $J_{nn',ss'}(k_y,q)=\frac{1}{2}(1+ss'\cos\theta)$, where θ is the angle between the vectors $(k_n,\ k_y+q)$ and $(k_{n'},\ k_y)$ [25].

An important feature is noted for the GNR Coulomb interaction at shorter distances. The integral in Eq. (9) is dominated by the transitions $n=n'$, $m=m'$, giving $v(q)=\mathrm{v}^R(q)\equiv v_{nn,n'n'}(q)/(\mathrm{w}^2)\approx e^2[3-2\gamma-2\ln(q\mathrm{w}/2)]$. Thus summing the bubble diagrams result in the same expression for the RPA response as in Eq. (4) with $\chi_0(q,\omega)=\sum_{nn',ss'}\chi_0^{nn',ss'}(q,\omega)$, and with the Coulomb potential being $\mathrm{v}^R(q)$.

Quantum dispersion forces for GNRs.—To calculate the GNR interaction, $\mu=0$ and $T\to 0$ is considered first. The response is then due to the interband transitions (between $s=+$ and $-$), and the vdW force is determined by larger frequency excitations. As a result, the sum over ω_l in Eq. (6) becomes an integral, $\sum_l\to[\hbar/(2\pi k_BT)]\int_0^\infty d\omega$. Obtaining explicitly the distance dependence in f becomes possible using the interband polarization

$$\chi_0^{\mathrm{inter}}(q,\omega)=-\sum_n\frac{2v_0}{\hbar}q^2\int_0^{\pi/(\sqrt{3}a)}\frac{dk_y}{\pi}\times\frac{k_n^2}{(k_n^2+k_y^2)^{3/2}}\frac{1}{4v_0^2(k_n^2+k_y^2)-\omega^2}, \tag{11}$$

where n sums the low energy bands for which the model for Eq. (7) is valid. Figure (2) shows the interband conductivity for two narrow ribbons, where $\sigma^{\mathrm{inter}}(q,\omega)=ie^2\omega\chi_0^{\mathrm{inter}}(q,\omega)/q^2$. Note the shift in the conductivity peaks towards smaller frequencies as the GNR width increases. Using Eq. (6), the vdW force between the ribbons is calculated as

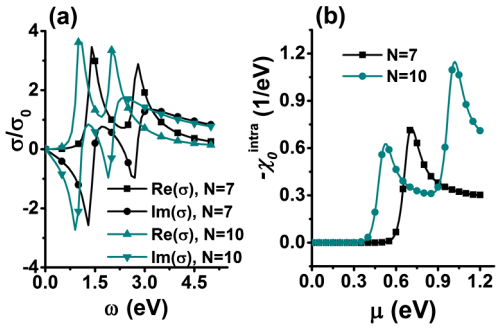

FIG. 2 (color online). (a) Real and imaginary parts of the conductivity σ, in units of $\sigma_0 = ae^2/\hbar$, vs frequency for two armchaired GNRs with $N = 7, 10$. (b) The magnitude of χ_0^{intra} vs μ for armchaired GNRs with $N = 7$, 10, and $T = 300$ K.

$$f = -\frac{A}{a^2}\left(\frac{a}{d}\right)^6, \tag{12}$$

where $A = 0.035$ eV for $N = 7$ and $A = 0.092$ eV for $N = 10$. The constant A depends on the particular ribbon and it increases as N increases. The vdW force was also calculated via dielectric response in which the tight binding energies without the long wavelength approximation was used [26]. We note that the characteristic behavior of the force is preserved and the results do not differ significantly from those found by Eq. (12).

We compare these findings with the calculations in Table I. It is seen that the distance dependence of the vdW interaction between GNRs is the same as that of a typical 1D dielectric. This behavior is essentially due to the presence of a relatively large energy gap in the band structure of the ribbons. We also note that the tight-binding model in Eq. (7) is suitable for GNR separations ~50 nm or larger. For shorter distances, a more complete energy band structure is needed to account for higher optical transitions, as it has been shown for the interaction between graphene layers [27].

The chemical potential and thermal effects.—Switching on the chemical potential μ and raising the temperature has important effects on the GNR response. As μ is increased to $\sim E_g/2$, the effect from the interband transitions at room temperature becomes small compared to the low frequency intraband response. At low ω, high T, and large μ, one obtains

$$\chi_0^{\text{intra}}(q) \approx -2\sum_n \frac{1}{k_B T}\int_0^{\pi/(\sqrt{3}a)} \frac{dk_y}{\pi} \times \frac{\cosh(|E_n|/k_BT)\cosh(\mu/k_BT)+1}{[\cosh(\mu/k_BT)+\cosh(|E_n|/k_BT)]^2}. \tag{13}$$

Figure (2) shows that at $\mu \sim E_g/2 \approx 0.7$ eV ($N = 7$) and $\mu \sim E_g/2 \approx 0.5$ eV ($N = 10$), χ_0^{intra} experiences a large increase completely dominating the GNR response. The critical point where that happens is when μ corresponds to the energy at the bottom of the lowest conduction band, while the second peak in the interaction for $N = 10$ occurs when μ corresponds to the energy at the bottom of the second lowest conduction band.

The much enhanced low frequency, intraband response, and suppressed high frequency interband response at larger temperatures affects the interaction significantly. More specifically, the quantum mechanical contribution in the vdW force is overtaken by the thermal fluctuations given by the $l = 0$ term in Eq. (6):

$$f_T = -k_B T \int_0^\infty \frac{qdq}{\pi}\frac{K_1(qd)}{K_0(qd)}\frac{[v(q,d)\chi_0^{\text{intra}}(q)]^2}{[1-v(q)\chi_0^{\text{intra}}(q)]^2}, \tag{14}$$

where K_1 is the first-order modified Bessel function of the second kind. The significant enhancement of f_T as a function of μ is shown in Fig. 3(a), which correlates with the increase in χ_0^{intra} vs μ from Fig. 2(b).

f_T is further analyzed to understand how the specific forms of the Coulomb potential and the GNR response function χ_0^{intra} influence the force. One notes that when χ_0^{intra} is large, ρ_B [Eq. (6)] can be approximated as $\rho_B \approx 1$. Taking $v(q) = \mathrm{v}^0(q) \equiv -2e^2 \ln(|q|\mathrm{w})$, an analytical expression for f_T is derived (Table I). The log-log plot in Fig. 3(b) shows that the analytical formula has a similar behavior as the numerically calculated f_T using Eq. (6) with $\rho_B = 1$. It turns out that taking the Coulomb potential for the GNR $\mathrm{v}^R(q) = e^2[3 - 2\gamma + \ln(4) - 2\ln(|q|\mathrm{w})]$ instead of $\mathrm{v}^0(q)$ or keeping χ_0^{intra} explicitly in ρ_B affects the force significantly. Although the calculated log-log dependence is approximately linear in all cases, the slopes and intercepts are different. Our numerical calculations show that $f_T a^2 \approx -0.000163(a/d)^{2.26}$ [eV] for $\rho_B(\chi_0^{\text{intra}})$ and $\mathrm{v}^R(q)$,

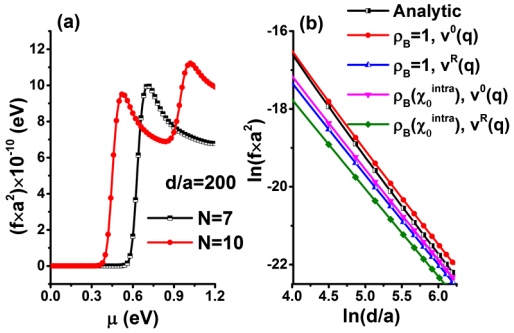

FIG. 3 (color online). (a) Magnitude of thermal vdW force between two GNRs ($N = 7, N = 10$ carbon lines) vs the chemical potential at $T = 300$ K. (b) Log-Log plot of the 1D thermal vdW force vs scaled d/a separation at $T = 300$ K. χ_0^{intra} is used for armchair GNRs with $N = 7$. Also, $f \times a^2$ is in units of eV. Estimated power laws: (analytic) $\rightarrow fa^2 = 0.00144(a/d)^{2.53}$, $[\rho_B = 1, \mathrm{v}^0(q)] \rightarrow fa^2 = 0.00116(a/d)^{2.46}$, $[\rho_B = 1, \mathrm{v}^R(q)] \rightarrow fa^2 = 0.000308(a/d)^{2.32}$, $[\rho_B(\chi_0^{\text{intra}}), \mathrm{v}^0(q)] \rightarrow fa^2 = 0.000407(a/d)^{2.35}$), $[\rho_B(\chi_0^{\text{intra}}), \mathrm{v}^R(q)] \rightarrow fa^2 = 0.000163(d/a)^{2.26}$.

while $f_T \approx -0.00116(a/d)^{2.46}$ [eV] for $\rho_B(\chi_0^{\text{intra}}) = 1$ and $v^0(q)$. Other estimates are shown in the figure.

We remark that in regular 3D dielectrics and metals, thermal effects in the vdW force are usually very small, because the dielectric response at low ω is much smaller as compared to the one for large ω. As a result, Matsubara frequencies with large l, characteristic for the quantum mechanical regime, dominate the interaction. Graphitic nanostructures allow for unprecedented opportunities to access the previously unavailable thermal fluctuations regime in a modulating fashion. It was shown in recent studies [6] that the graphene vdW force is always thermal at separations $d > 50$ nm - $F_T = -k_B T/(8\pi d^3)$. Note that F_T is the same as the one for two 3D half-spaces; thus, the 2D nature does not play a role in obtaining this characteristic behavior. For GNRs, however, one can tune the vdW thermal effects upon changing μ as the dimensionality is crucial for the unique distance behavior [Table I, Fig. (3)].

This type of control of the vdW thermal effects via the chemical potential is also possible for carbon nanotubes. Although the quantization occurs due to the zone folding around the circumference, the carbon nanotube response properties exhibit similar behavior in terms of inter- and intraband transitions [28] affected by μ as the ones for the GNRs. We also consider GaAs quantum wires, which are typical narrow 1D structures [29] with a response function $\chi(q,\omega) = \omega_p^2(q)/[\omega^2 - \omega_p^2(q)]$, with plasma frequency $\omega_p^2(q) \sim (2n_{1D}e^2/m)q^2|\ln(q\mathrm{w})|$ and corresponding Coulomb potential $v(q) = 2e^2(|\ln(q\mathrm{w})| + 1.972\ldots)$. At $T = 0$, using Eq. (6) one finds that the vdW force is similar to the one for a metallic wire (Table I). As T is increased, the long wavelength plasmon dispersion does not change significantly [29] and the force is completely dominated by the $l = 0$ Matsubara term (thermal, Table I). This can be understood by comparing the relevant analytical expressions for the force in Table I, showing that $\hbar\omega_{p,0}(\mathrm{w}/d) \ll k_B T$, where $\omega_{p,0}^2 = 2n_{1D}e^2/m\mathrm{w}^2$. Since $\omega_{p,0}$ is much reduced than the bulk plasma frequency [29], the thermal vdW force is dominant in such wires at room temperature. It should also be noted that as the width of the graphene nanoribbons becomes larger, thermal effects become more significant even for low chemical potential.

Conclusion.—In summary, a Lifhsitz-like formula for the vdW force, derived using RPA, between 1D materials is presented and applied to GNRs and some typical materials. The detailed calculations of the nanoribbon response properties allowed us to uncover the possibility for quantum mechanical to thermal transitions. The GNR optical properties tunability enables the onset of such effects in quasi-1D systems, which can be used to access previously unattainable regimes in vdW forces in most typical 3D materials.

We acknowledge financial support from the Department of Energy under Contract No. DE-FG02-06ER46297.

[1] K. S. Novoselov, V. I. Fal'ko, L. Colombo, P. R. Gellert, M. G. Schwab, and K. Kim, Nature (London) **490**, 192 (2012).
[2] N. Koratkar, *Graphene in Composite Materials; Synthesis, Characterization, and Applications* (DEStech Publications, Lancaster, Pennsylvania, 2013)
[3] H. Rydberg, M. Dion, N. Jacobson, E. Schröder, P. Hyldgaard, S. I. Simak, D. C. Langreth, and B. I. Lundqvist, Phys. Rev. Lett. **91**, 126402 (2003).
[4] A. Tkatchenko and M. Scheffler, Phys. Rev. Lett. **102**, 073005 (2009).
[5] S. Lebègue, J. Harl, T. Gould, J. G. Ángyan, G. Kresse, and J. F. Dobson, Phys. Rev. Lett. **105**, 196401 (2010).
[6] G. Gómez-Santos, Phys. Rev. B **80**, 245424 (2009).
[7] G. L. Klimchitskaya and V. M. Mostepanenko, Phys. Rev. B **87**, 075439 (2013).
[8] V. Svetovoy, Z. Moktadir, M. Elwenspoek, and H. Mizuta, Europhys. Lett. **96**, 14006 (2011).
[9] B. E. Sernelius, Europhys. Lett. **95**, 57003 (2011).
[10] D. Drosdoff, A. D. Phan, L. M. Woods, I. V. Bondarev, and J. F. Dobson, Eur. J. Phys. B **85**, 365 (2012).
[11] A. A. Banishev, H. Wen, J. Xu, R. K. Kawakami, G. L. Klimchitskaya, V. M. Mostepanenko, and U. Mohideen, Phys. Rev. B **87**, 205433 (2013).
[12] L. Ma, J. Wang, and F. Ding, ChemPhysChem **14**, 47 (2013).
[13] X. Wang, Y. Ouyang, X. Li, H. Wang, J. Guo, H. Dai, Phys. Rev. Lett. **100**, 206803 (2008).
[14] J. F. Dobson, A. White, and A. Rubio, Phys. Rev. Lett. **96**, 073201 (2006).
[15] J. F. Dobson, T. Gould, and I. Klich, Phys. Rev. A **80**, 012506 (2009).
[16] E. Noruzifar, T. Emig, U. Mohideen, and R. Zandi, Phys. Rev. B **86**, 115449 (2012).
[17] A. O. Sushkov, W. J. Kim, D. A. R. Dalvit, and S. K. Lamoreaux, Nat. Phys. **7**, 230 (2011).
[18] G. L. Klimchitskaya, M. Bordag, E. Fishbach, D. E. Krause, and V. M. Mostepanenko, Int. J. Mod. Phys. A **26**, 3918 (2011).
[19] E. M. Lifshitz, Sov. Phys. JETP-USSR **2**, 73 (1956).
[20] A. A. Abrikosov, L .P. Gorkov, and I. E. Dzyaloshinski, *Methods of Quantum Field Theory in Statistical Physics* (Dover, New York, 1975), Chap. 3.
[21] T. Ando, A. Fowler, and F. Stern, Rev. Mod. Phys. **54**, 437 (1982).
[22] S. Das Sarma and E. H. Hwang, Phys. Rev. Lett. **102**, 206412 (2009).
[23] L. Brey and H. A. Fertig, Phys. Rev. B **75**, 125434 (2007).
[24] M. Y. Han, B. Özyilmaz, Y. Zhang, and P. Kim, Phys. Rev. Lett. **98**, 206805 (2007).
[25] L. Brey and H. A. Fertig, Phys. Rev. B, **73**, 195408 (2006).
[26] K. I. Sasaki, K. Kato, Y. Tokura, K. Oguri, and T. Sogawa, Phys. Rev. B **84**, 085458 (2011).
[27] D. Drosdoff and L. M. Woods, Phys. Rev. A **84**, 062501 (2011).
[28] S. Rech, C. Thomsen, and J. Maultzsch, *Carbon Nanotubes, Basic Concepts and Physical Properties* (Wiley-VCH, Weinheim, 2004).
[29] Ben Yu-Kuang Hu and S. Das Sarma, Phys. Rev. B **48**, 5469 (1993); S. Das Sarma, E. H. Hwang, and L. Zheng, Phys. Rev. B **54**, 8057 (1996); T. Vazifehshenas and S. Ghasem, Eur. Phys. J. B **65**, 225 (2008).